Respective dependencies of conventional and spontaneous exchange biases on spin glass

Pei Liu,[1,*] Bing Lv,[1,*] Yongzuo Wang,[1] Peng Chen,[1] Lei Wang,[2,†] and Cunxu Gao[1,‡]

[1]*Key Laboratory for Magnetism and Magnetic Materials of the Ministry of Education, Lanzhou University, Lanzhou 730000, People's Republic of China*

[2]*Key Laboratory of Quantum Materials and Devices of Ministry of Education, School of Physics, Southeast University, Nanjing 211189, People's Republic of China*

(Received 17 November 2023; revised 9 April 2024; accepted 22 April 2024; published 6 May 2024)

A conventional exchange bias manifests itself as a hysteresis loop shift in systems with an interface between a ferromagnet and an antiferromagnet after field cooling. Due to the complicated magnetic interactions at the interface, a spin glass with disordered and frustrated spin configurations is generated, resulting in the dependencies of the conventional exchange bias mechanism on a spin glass still being elusive. Here, we report that a spin glass, CuMn, exhibits a conventional exchange bias as in interface magnetic systems. More importantly, a spontaneous exchange bias is also observed in the spin glass after zero-field cooling, which is attributed to the response of ferromagnetic clusters embedded in a spin-glass matrix at high magnetic fields that form a unidirectional anisotropy through the interaction between the clusters and the spin-glass matrix. Our results show the relationship between the exchange bias and spin glasses, offering a foundational understanding for exchange bias research.

DOI: 10.1103/PhysRevB.109.184412

I. INTRODUCTION

The exchange bias effect is a subject of great academic and technological interest [1]. Usually, this effect is ascribed to the unidirectional magnetic anisotropy formed at the interfaces of antiferromagnetic and ferromagnetic phases in heterogeneous systems. It can be observed after the heterogeneous system is cooled through its Néel temperature under an applied magnetic field, which we refer to as conventional exchange bias (CEB) [2,3]. Later, Wang *et al.* obtained a spontaneous exchange bias (SEB) effect in NiMnIn alloys at low temperatures under a zero-field-cooling condition [4]. Since there is no need for an additional cooling field to induce unidirectional anisotropy in this condition, the SEB devices are more easily manipulated by the electric field and have more practical application value [3,5]. Despite decades of study of the exchange bias effect and its wide application, its underlying mechanism still remains elusive due to competing magnetic interactions with undefined magnetic interfaces between two different magnetic phases [6,7]. One of the key points that has emerged is the role of frustration and disorder at the interface, which is of fundamental importance for magnetic glass states [8–10].

A spin glass typically appears when magnetic atoms are randomly diluted with frustrated magnetic order in a nonmagnetic metallic host. As the spatial distribution of the spins is random, the long-range oscillatory nature of the Ruderman-Kittel-Kasuya-Yoshida (RKKY) interaction between the spins prevents the system from exhibiting long-range ferromagnetic or antiferromagnetic order, but may induce a new phase where the spins are frozen in random directions at low temperatures [11–13]. In these systems, unidirectional anisotropy appears in field-cooled or zero-field-cooled samples at temperatures well below the cusp temperature of the zero-field-cooled magnetization curve [14–16]. Recently, the exchange bias observed in compound systems [17,18] was also found, accompanied with the emergence of the spin-glass phase. However, the relationship between the exchange bias and spin glass is unclear [19]. Here, we report results from experiments on $Cu_{100-x}Mn_x$ ($x = 5, 8, 11, 14, 17, 20$) films where we have only used a canonical example of a spin glass that replicated the CEB and SEB phenomena, clarifying the relationship between the exchange bias and spin glass to be the case.

II. EXPERIMENT

The $Cu_{100-x}Mn_x$ films were epitaxially grown on Si(111) substrates by molecular beam epitaxy. Prior to growth, the Si(111) substrates were chemically cleansed, heat treated, and then transferred to the deposition chamber. The substrates were further thermally cleansed at a temperature of 700 °C for 1 h with a base pressure of $\sim 10^{-7}$ Pa to remove the surface hydroxide and obtain a Si(111)7×7 reconstruction. After cooling the substrate temperature down to room temperature, 3-nm-thick Cu was deposited on the substrate, and then the films of CuMn were prepared with a thickness of 30 nm. Finally, 3-nm-thick Al was capped to prevent oxidation in the air. A quartz microbalance was employed *in situ* to obtain the chemical composition of the sample. The film growth rates of Mn and Cu sources were also separately calibrated by *ex situ* x-ray reflectivity (XRR). The CEB and SEB were studied in a series of $Cu_{100-x}Mn_x$ samples by the superconducting quantum interference device of a magnetic

*These authors contributed equally to this work.
†wanglei.icer@seu.edu.cn
‡gaocunx@lzu.edu.cn

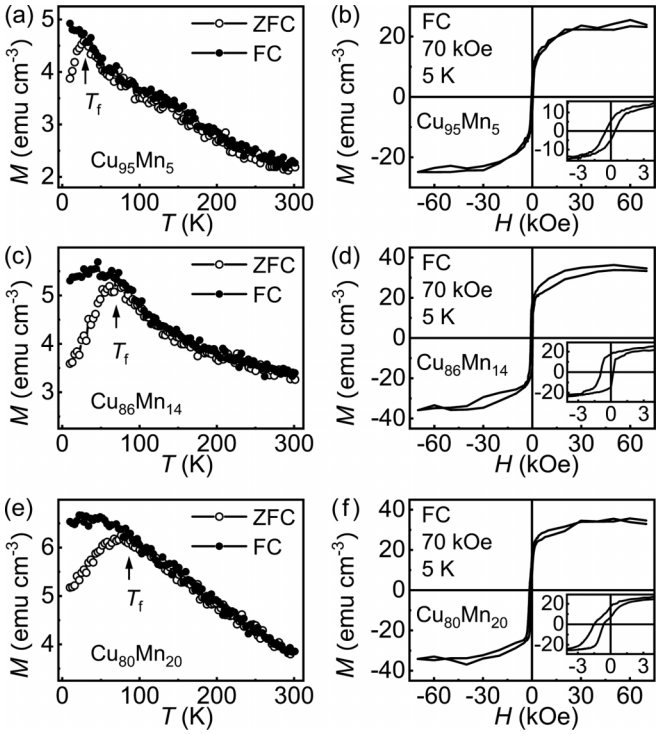

FIG. 1. The temperature dependence of magnetization following ZFC and FC measurements at 1 kOe for (a) $Cu_{95}Mn_5$, (c) $Cu_{86}Mn_{14}$, and (e) $Cu_{80}Mn_{20}$. The temperature at which FC and ZFC branches meet is marked by T_f. $M(H)$ loops at 5 K after FC ($H = 70$ kOe) from 300 K for (b) $Cu_{95}Mn_5$, (d) $Cu_{86}Mn_{14}$, and (f) $Cu_{80}Mn_{20}$. The insets present an expanded view of the main plot (same units) close to the origin, showing a shifting along the field axis.

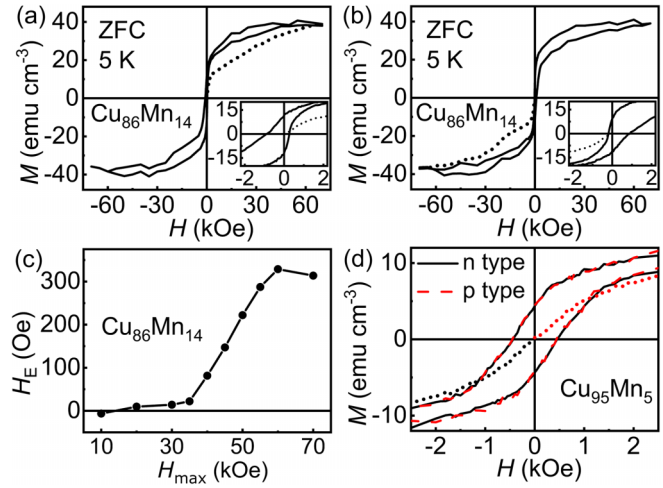

FIG. 2. The $M(H)$ loops of the $Cu_{86}Mn_{14}$ at 5 K with $H_{max} = 70$ kOe obtained from (a) the *p*-type sweep protocol and (b) *n*-type protocol hysteresis loops are shown. The dotted lines show the initial magnetization curves. The insets present an expanded view of the main plot (same units) close to the origin. (c) H_E as a function of H_{max} in CuMn at 5 K after ZFC. (d) Zoom-in on $M(H)$ loops of the $Cu_{95}Mn_5$ at 5 K with $H_{max} = 70$ kOe, both *p*-type and *n*-type sweep protocols were performed. Before measuring each $M(H)$ loop, the sample was warmed up to 200 K well above T_f to negate the magnetic memory effect.

property measurement system (MPMS XL-7). We define the exchange bias field, $H_E = -(H_{c+} + H_{c-})/2$, as the offset of the hysteresis loop along the field axis, where H_{c-} and H_{c+} are the left and right coercive fields of magnetic hysteresis loops, respectively.

III. RESULTS AND DISCUSSION

The temperature dependence of dc magnetization $M(T)$ after zero-field cooling (ZFC) and field cooled (FC) for CuMn with varying Mn content is shown in Figs. 1(a), 1(c), and 1(e). For FC measurements, the sample was cooled above freezing temperature T_f to the target temperature with a cooling field of 70 kOe. In CuMn films, FC and ZFC curves begin to separate, which indicates the presence of a frozen moment and suggests a freezing temperature T_f [20,21]. Comparing the magnetization curves of the present samples shown in Figs. 1(a), 1(c), and 1(e), the samples show that the freezing temperature gradually increases with increasing Mn concentration, in agreement with previous reports [22,23]. We illustrate the low-temperature hysteresis loops taken at 5 K for samples ($x = 5$, 14, and 20) cooled in 70 kOe in Figs. 1(b), 1(d), and 1(f), respectively. In each case, the presence of a large shift in the loop along the field axis is conspicuous. In addition, the hysteresis loops in the samples with $x = 8$, 11, and 17 also show a shift along the field axis (not shown here). As a result, the CEB phenomenon was observed in all CuMn samples, consistent with the reported results [24,25]. Meanwhile, the CEB turns out to be negative, i.e., cooling under the positive field yields a hysteresis loop shift in a negative direction along the field axis.

In order to investigate the behavior of SEB, two measuring processes were used to measure the hysteresis loops after ZFC: One is a *p*-type condition where the initial magnetic field starts from zero and increases to a positive value, and the other is an *n*-type condition where the initial magnetic field starts from zero and increases to a negative value. Generally, these two kinds of measurements will yield the same loop except for the initial magnetization curve [4]. However, for SEB they will be different, which has been reported previously [3]. Figure 2(a) shows the *p*-type $M(H)$ loop of $Cu_{86}Mn_{14}$ at 5 K after ZFC from 300 K with a maximum measurement field $H_{max} = 70$ kOe. The dotted lines show the initial magnetization curves, which lie outside the hysteresis loop. The magnetization at the starting point of the initial magnetization curve is close to zero, indicating that the initial state of the sample is an unmagnetized state or of very low magnetization. This result rules out the naive explanation of the remnant field of a superconductor magnet or remanent magnetization of the sample [26,27]. Meanwhile, as shown in Fig. 2(b), we measured the *n*-type $M(H)$ loop of $Cu_{86}Mn_{14}$ at 5 K after ZFC, where the loop shifts to the positive magnetic field axis. Furthermore, as the magnetic field increases to positive and negative maxima in both *p*-type and *n*-type measurements, the magnetization values tend to be consistent, indicating that the shifted loop is not a minor loop. Simultaneously, it is worth noting that in previous reports, CuMn alloys with a Mn element content around 14% had not shown shifted hysteresis loops after ZFC [28–30].

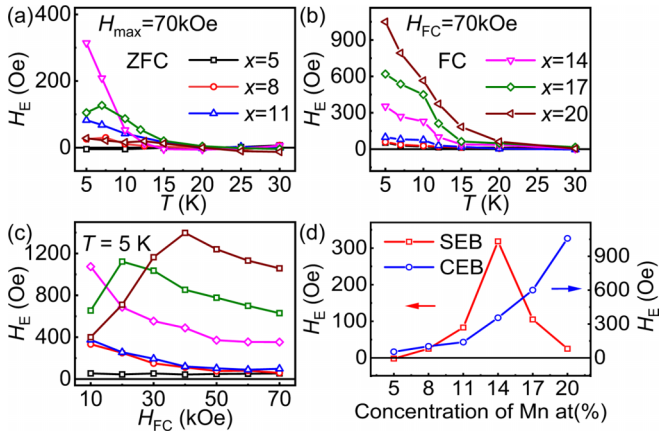

FIG. 3. (a) Temperature dependence of the H_E for CuMn films with $H_{max} = 70$ kOe after ZFC. (b) Temperature dependence of the H_E for CuMn films with $H_{FC} = 70$ kOe after FC from 200 K. (c) H_E vs H_{FC} for CuMn films, measured at 5 K. (d) H_E of SEB ($H_{max} = 70$ kOe) and CEB ($H_{FC} = 70$ kOe) as a function of Mn content at 5 K. The solid lines are guides for the eyes.

In order to prove the authenticity of our data and understand the magnetic properties, we further measured the *p*-type hysteresis loops of the $Cu_{86}Mn_{14}$ at 5 K after ZFC from well above the freezing temperature with different maximum measurement fields H_{max}, i.e., when measuring the hysteresis loops, the field varies as follows: $0 \rightarrow H_{max} \rightarrow 0 \rightarrow -H_{max} \rightarrow 0 \rightarrow H_{max}$. Figure 2(c) shows the H_{max} dependence of the exchange bias field H_E. There is a certain value H_{max} at which H_E changes from zero to nonzero and gradually increases with increasing H_{max}, suggesting that magnetic fields above a certain field should be used when measuring SEB in dilute magnetic systems. Furthermore, we can exclude the possibility that the shifts of the magnetic hysteresis loops along the field axis are the minor loop effect in our experiment. For minor hysteresis loops, the shift is expected to decrease as the sweeping field increases [31], which is the opposite of what we observe [Fig. 2(c)]. On the contrary, during both *p*-type and *n*-type measurements of the $Cu_{95}Mn_5$ sample after ZFC, the magnetic hysteresis loops excluding the initial magnetization curve tend to be consistent, i.e., there is no exchange bias in the $Cu_{95}Mn_5$ sample, as shown in Fig. 2(d). This result shows that SEB is not only related to the glassy state in materials, but that other unknown factors also play a crucial role in the formation of SEB.

To understand the origin of the exchange bias, the temperature and cooling field dependence of the exchange bias field H_E have been studied, as shown in Fig. 3. The enhancement of magnetic irreversibility below the freezing temperature after ZFC in the CuMn spin glass results in the increase of H_E in Fig. 3(a). We notice that the H_E of the CuMn with the lowest content of Mn elements after ZFC has almost zero values at low temperatures, e.g., the $Cu_{95}Mn_5$ sample does not display the SEB phenomenon. As the Mn content in the alloy increases, the H_E of the sample at low temperature gradually increases until it reaches 14%, as shown in Fig. 3(a). However, as the Mn content continues to increase, the H_E tends to decrease instead. Figure 3(b) shows that all samples have nonzero H_E values at low temperatures after FC. The H_E values of high Mn content samples are larger than those of the low Mn content ones, implying that the CEB behavior is associated with disordered and frustrated magnetic order. Meanwhile, the H_E of samples after ZFC and FC reduces rapidly with increasing temperature and becomes negligible above their blocking temperatures, indicating that the strength of the thermal potential energy exceeds the unidirectional anisotropy [32,33].

CEB is thought to be driven by a disordered spin configuration at the ferromagnetic-antiferromagnetic interface, where uncompensated moments are pinned by the antiferromagnetic phase [9,34]. Here, Fig. 3(c) shows the cooling field (H_{FC}) dependence of the H_E in the CuMn spin glass. For the samples with a Mn concentration below 14%, there is a continuous decrease of H_E with H_{FC} up to 70 kOe, while for $x = 17$ and 20, H_E increases first and then decreases with the increase of cooling field. For CEB, the different dependence behaviors of H_E on H_{FC} for high and low Mn concentrations could be ascribed to the intensity of unidirectional anisotropy. This unidirectional anisotropy is caused by the interaction between the clusters and spin-glass matrix. For low Mn concentration, the weak field is enough to rotate the frozen spin in a spin-glass matrix, and thus to deteriorate the unidirectional anisotropy. Therefore, the H_E decreases with increasing field. For a high Mn content of $x = 17$ and 20, the weak field cannot rotate the localized frozen clusters due to a large anisotropy, thus, a stronger field can induce a stronger unidirectional anisotropy and the H_E will increase with field. While the unidirectional anisotropy reaches a maximum, H_E will decrease with the increasing field again, just as in the situation with low Mn content. Other factors such as the magnetic field may have the possibility to induce an increase or decrease of the size of the clusters, providing a similar effect as the Mn concentration.

Figure 3(d) shows the Mn content dependence of H_E in two types of EB at 5 K. The strength of CEB increases with an increase of Mn content in the alloy, which is consistent with the trend of freezing temperature T_f with Mn content in CuMn spin glasses [35]. The higher CEB obtained for samples with a higher Mn content suggests that the CEB is related to disordered and frustrated spin configuration in the spin glass. In contrast, Fig. 3(d) shows a nonmonotonic correlation between the presence of SEB and Mn content. The Mn content dependence of H_E exhibits a maximum at $x = 14$ for SEB. However, the H_E in $Cu_{95}Mn_5$ after ZFC is nearly zero, i.e., there is some hidden factor that plays an important role in the formation of SEB.

To dispel the uncertainty regarding the formation of SEB, a microcosmic view of the spin structure of the alloys is needed. Thus, we set up a $28 \times 28 \times 28$ supercell of the CuMn alloys and carry out Monte Carlo (MC) calculations to calculate their corresponding ground states after cooling. Technically, the MC calculations are realized by an open source code UPPASD [36,37], where the long-range RKKY interactions dominated by the Hamiltonian of the CuMn alloy are categorized as [38]

$$\mathcal{H}_{ij} = -\mathcal{A}\mathbf{S}_i\mathbf{S}_j \cos(2k_F r_{ij})/r_{ij}^3, \quad (1)$$

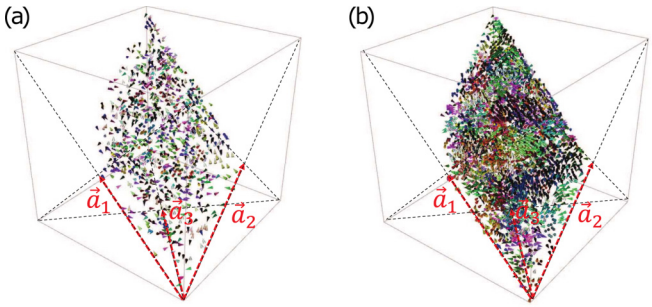

FIG. 4. The spin textures obtained by Monte Carlo (MC) calculations for $Cu_{95}Mn_5$ (a) and $Cu_{80}Mn_{20}$ (b) around 5 K, where the spins form a canonical spin-glass state in $Cu_{95}Mn_5$ and ferromagnetic clusters in $Cu_{80}Mn_{20}$, respectively.

with i, j representing any two nonequivalent spins in the system, $\mathcal{A} = 2.94 \times 10^4$ K standings for the coupling parameter, $k_F = 1.35$ Å^{-1} being the free-electron Fermi vector of Cu, $\mathbf{S}$ denoting the direction of the spins, and r_{ij} is the the corresponding distance between spin i and j. For the cooling process, the initial temperature is set to be $T_0 = 800$ K and we cool down the system step by step with $T_n = T_0\chi^n$ (step $n \in [1, 15]$, cooling rate $\chi \simeq 0.7129$) to obtain the ground states of CuMn alloys around 5 K. Moreover, the semi-implicit midpoint solver with a time step of $\tau = 10^{-16}$ s and 20 000 MC circles are used to converge the results for any T_n. Finally, the spin texture of $Cu_{95}Mn_5$ and $Cu_{80}Mn_{20}$ are shown in Figs. 4(a) and 4(b), respectively.

In $Cu_{95}Mn_5$ as shown in Fig. 4(a), the random location of the single Mn moments and the long-range oscillatory nature of the RKKY exchange interaction prevent the system from exhibiting long-range ferromagnetic or antiferromagnetic order but induce a new magnetic phase called a canonical spin glass (CSG), in which the spins are frozen in random directions [39,40]. However, when the Mn content continues to increase above the percolation limit, it leads to the growth of ferromagnetic clusters as reported [41,42]. In other words, there is a nonzero probability that a given occupied site belongs to an unbounded cluster when the concentration is above the percolation limit. As a consequence, the CSG state in CuMn alloys gradually disappears, and the ferromagnetic clusters can no longer be separated from each other in the CSG matrix, which corresponds to the $Cu_{80}Mn_{20}$ sample in our work as shown in Fig. 4(b). In this sense, there should be a transition state between the above two states, where the corresponding spins have a greater statistical chance of the Mn atom being the first or second nearest neighbor to another Mn atom, i.e., some of the Mn atoms can strongly couple with neighboring Mn atoms and build themselves into localized clusters with ferromagnetic short-range correlations [14,43]. Consequently, the magnetic behavior of CuMn alloys refers to stable ferromagnetic clusters embedded in a CSG matrix [22], corresponding to the $Cu_{86}Mn_{14}$ sample in our work.

Under this transition state, only the single Mn atoms in a CSG matrix respond to the external magnetic field when a small field (H_{max}) is applied to the measured hysteresis loop after ZFC, while the nonpercolating ferromagnetic clusters remain frozen in the random direction due to their large anisotropy. If H_{max} is increased, it becomes possible to rotate the spins in the ferromagnetic clusters during the initial magnetization process, rotating their net moments to the field direction and thereby contributing to the overall magnetism. The magnetization will be only reversed as the reverse magnetic field increases enough to overcome the coupling energy between the ferromagnetic clusters and the CSG matrix. Meanwhile, a unidirectional anisotropy is formed by the interaction between localized clusters and CSG during the initial magnetization process below the blocking temperature after ZFC.

As a result, both the CSG and the ferromagnetic clusters contribute to the SEB, and the absence of one magnetic phase reduces or even eliminates the SEB phenomenon. As shown in Fig. 3(d), the strength of SEB decreases as Mn content increases above the percolation limit. In the case of low Mn content, only the CSG magnetic phase exists in CuMn alloys, and the SEB disappears accordingly. The experimental results show that the SEB is driven by the coupling formed between ferromagnetic clusters and the surrounding spin-glass phase during the initial magnetization after ZFC, and the CEB is intertwined with the glassy state. But we notice that the CEB is also described as a ferromagnetic unidirectional anisotropy formed at the interface between different magnetic phases [44,45].

IV. CONCLUSION

In summary, we investigated both SEB and CEB effects in a conventional spin-glass system. The experimental results show that the existence of CEB is consistent with the existence of glassy behavior caused by spin frustration and disorder at the interface region. Meanwhile, the SEB effect is attributed to the unidirectional anisotropy formed by multiple magnetic phases in the material during the initial magnetization process. The SEB is weakened or even disappears in a glassy state that is dominated by one magnetic phase. In principle, these results provide an example for understanding of the CEB and SEB effects in magnetic materials with the help of a spin glass.

ACKNOWLEDGMENTS

This work was supported by the National Natural Science Foundation of China (Grant No. 12074157), Gansu Key Research and Development Program under (Grant No. 23YFGA0008), and the Fundamental Research Funds for the Central Universities (Grant No. lzujbky-2022-kb06).

[1] P. K. Manna and S. M. Yusuf, Two interface effects: Exchange bias and magnetic proximity, Phys. Rep. **535**, 61 (2014).

[2] A. K. Nayak, M. Nicklas, S. Chadov, C. Shekhar, Y. Skourski, J. Winterlik, and C. Felser, Large zero-field cooled exchange-bias in bulk Mn_2PtGa, Phys. Rev. Lett. **110**, 127204 (2013).

[3] S. Lin, D. F. Shao, J. C. Lin, L. Zu, X. C. Kan, B. S. Wang, Y. N. Huang, W. H. Song, W. J. Lu, P. Tong, and Y. P. Sun, Spin-glass behavior and zero-field-cooled exchange bias in a Cr-based antiperovskite compound $PdNCr_3$, J. Mater. Chem. C **3**, 5683 (2015).

[4] B. M. Wang, Y. Liu, P. Ren, B. Xia, K. B. Ruan, J. B. Yi, J. Ding, X. G. Li, and L. Wang, Large exchange bias after zero-field cooling from an unmagnetized state, Phys. Rev. Lett. **106**, 077203 (2011).

[5] F. Tian, K. Cao, Y. Zhang, Y. Zeng, R. Zhang, T. Chang, C. Zhou, M. Xu, X. Song, and S. Yang, Giant spontaneous exchange bias triggered by crossover of superspin glass in Sb-doped $Ni_{50}Mn_{38}Ga_{12}$ Heusler alloys, Sci. Rep. **6**, 30801 (2016).

[6] L. T. Coutrim, E. M. Bittar, F. Stavale, F. Garcia, E. Baggio-Saitovitch, M. Abbate, R. J. O. Mossanek, H. P. Martins, D. Tobia, P. G. Pagliuso, and L. Bufaiçal, Compensation temperatures and exchange bias in $La_{1.5}Ca_{0.5}CoIrO_6$, Phys. Rev. B **93**, 174406 (2016).

[7] Y. Xia, R. Wu, Y. Zhang, S. Liu, H. Du, J. Han, C. Wang, X. Chen, L. Xie, Y. Yang, and J. Yang, Tunable giant exchange bias in the single-phase rare-earth–transition-metal intermetallics $YMn_{12-x}Fe_x$ with highly homogenous intersublattice exchange coupling, Phys. Rev. B **96**, 064440 (2017).

[8] S. Gondh, M. M. Patidar, K. Kumar, M. P. Saravanan, V. Ganesan, and A. K. Pramanik, Large exchange bias and low-temperature glassy state in the frustrated triangular-lattice antiferromagnet $Ba_3NiIr_2O_9$, Phys. Rev. B **104**, 014401 (2021).

[9] E. Maniv, R. A. Murphy, S. C. Haley, S. Doyle, C. John, A. Maniv, S. K. Ramakrishna, Y.-L. Tang, P. Ercius, R. Ramesh, A. P. Reyes, J. R. Long, and J. G. Analytis, Exchange bias due to coupling between coexisting antiferromagnetic and spin-glass orders, Nat. Phys. **17**, 525 (2021).

[10] L. T. Coutrim, E. M. Bittar, F. Garcia, and L. Bufaiçal, Influence of spin glass-like magnetic relaxation on the zero-field-cooled exchange bias effect, Phys. Rev. B **98**, 064426 (2018).

[11] J. A. Mydosh, Spin glasses: redux: an updated experimental/materials survey, Rep. Prog. Phys. **78**, 052501 (2015).

[12] J. Kroder, K. Manna, D. Kriegner, A. S. Sukhanov, E. Liu, H. Borrmann, A. Hoser, J. Gooth, W. Schnelle, D. S. Inosov, G. H. Fecher, and C. Felser, Spin glass behavior in the disordered half-Heusler compound IrMnGa, Phys. Rev. B **99**, 174410 (2019).

[13] P. Bag, P. R. Baral, and R. Nath, Cluster spin-glass behavior and memory effect in $Cr_{0.5}Fe_{0.5}Ga$, Phys. Rev. B **98**, 144436 (2018).

[14] P. A. Beck, Comments on mictomagnetism, J. Less-Common Met. **28**, 193 (1972).

[15] L. C. Barnsley, E. M. Gray, and C. J. Webb, Asymmetric reversal in aged high concentration CuMn alloy, J. Phys.: Condens. Matter **25**, 086003 (2013).

[16] M. Hudl, R. Mathieu, and P. Nordblad, Tunable exchange bias in dilute magnetic alloys - chiral spin glasses, Sci. Rep. **6**, 19964 (2016).

[17] A. K. Singh, S. Chauhan, and R. Chandra, Antisite disorder induced spin glass and exchange bias effect in Nd_2NiMnO_6 epitaxial thin film, Appl. Phys. Lett. **110**, 102402 (2017).

[18] C. Macchiutti, J. R. Jesus, F. B. Carneiro, L. Bufaiçal, M. Ciomaga Hatnean, G. Balakrishnan, and E. M. Bittar, Absence of zero-field-cooled exchange bias effect in single crystalline $La_{2-x}A_xCoMnO_6$ (A = Ca, Sr) compounds, Phys. Rev. Mater. **5**, 094402 (2021).

[19] M. Ali, P. Adie, C. H. Marrows, D. Greig, B. J. Hickey, and R. L. Stamps, Exchange bias using a spin glass, Nat. Mater. **6**, 70 (2007).

[20] S. Pakhira, C. Mazumdar, R. Ranganathan, S. Giri, and M. Avdeev, Large magnetic cooling power involving frustrated antiferromagnetic spin-glass state in R_2NiSi_3 (R = Gd, Er), Phys. Rev. B **94**, 104414 (2016).

[21] S. Pal, K. Kumar, A. Banerjee, S. B. Roy, and A. K. Nigam, Field-cooled state of the canonical spin glass revisited, Phys. Rev. B **101**, 180402(R) (2020).

[22] P. Gibbs, T. M. Harders, and J. H. Smith, The magnetic phase diagram of CuMn, J. Phys. F: Met. Phys. **15**, 213 (1985).

[23] R. K. Chouhan and A. Mookerjee, Magnetic phase diagram for CuMn, J. Magn. Magn. Mater. **323**, 868 (2011).

[24] P. Monod, J. J. Prejean, and B. Tissier, Magnetic hysteresis of CuMn in the spin glass state, J. Appl. Phys. **50**, 7324 (1979).

[25] C. A. M. Mulder, A. J. van Duyneveldt, and J. A. Mydosh, Susceptibility of the CuMn spin-glass: Frequency and field dependences, Phys. Rev. B **23**, 1384 (1981).

[26] J. Geshev, Comment on: "Exchange bias and vertical shift in $CoFe_2O_4$ nanoparticles" [J. Magn. Magn. Mater. 313 (2007) 266], J. Magn. Magn. Mater. **320**, 600 (2008).

[27] L. Bufaiçal, L. T. Coutrim, E. M. Bittar, and F. Garcia, A phenomenological model for the spontaneous exchange bias effect, J. Magn. Magn. Mater. **512**, 167048 (2020).

[28] J. S. Kouvel, The ferromagnetic-antiferromagnetic properties of copper-manganese and silver-manganese alloys, J. Phys. Chem. Solids **21**, 57 (1961).

[29] J. A. Mydosh, Spin glasses and mictomagnets, AIP Conf. Proc. **24**, 131 (1975).

[30] P. A. Beck, Properties of mictomagnets (spinglasses), Prog. Mater. Sci. **23**, 1 (1980).

[31] J. Geshev, Comment on "Cluster glass induced exchange biaslike effect in the perovskite cobaltites" [Appl. Phys. Lett. **90**, 162515 (2007)], Appl. Phys. Lett. **93**, 176101 (2008).

[32] J.-I. Hong, T. Leo, D. J. Smith, and A. E. Berkowitz, Enhancing exchange bias with diluted antiferromagnets, Phys. Rev. Lett. **96**, 117204 (2006).

[33] M.-H. Phan, J. Alonso, H. Khurshid, P. Lampen-Kelley, S. Chandra, K. Stojak Repa, Z. Nemati, R. Das, Ó. Iglesias, and H. Srikanth, Exchange bias effects in iron oxide-based nanoparticle systems, Nanomaterials **6**, 221 (2016).

[34] F. Radu, A. Westphalen, K. Theis-Bröhl, and H. Zabel, Quantitative description of the azimuthal dependence of the exchange bias effect, J. Phys.: Condens. Matter **18**, L29 (2006).

[35] N. A. Gokcen, The Cu-Mn (copper-manganese) system, J. Phase Equilib. **14**, 76 (1993).

[36] B. Skubic, J. Hellsvik, L. Nordström, and O. Eriksson, A method for atomistic spin dynamics simulations:

implementation and examples, J. Phys.: Condens. Matter **20**, 315203 (2008).
[37] https://github.com/UppASD.
[38] W. Y. Ching and D. L. Huber, Thermodynamic properties of a classical RKKY model of CuMn, J. Phys. F: Met. Phys. **8**, L63 (1978).
[39] P. J. Ford, Spin glasses, Contemp. Phys. **23**, 141 (1982).
[40] C. Y. Huang, Some experimental aspects of spin glasses: A review, J. Magn. Magn. Mater. **51**, 1 (1985).
[41] E. M. Gray, T. J. Hicks, and J. H. Smith, Small-angle neutron scattering from a concentrated CuMn spin glass, J. Phys. F: Met. Phys. **12**, L189 (1982).
[42] F. Jiménez-Villacorta, D. Heiman, J. L. Marion, and L. H. Lewis, Tailored exchange in binary manganese—noble metal alloys, IEEE Magn. Lett. **4**, 1000204 (2013).
[43] J. A. Mydosh, Spin glasses—recent experiments and systems, J. Magn. Magn. Mater. **7**, 237 (1978).
[44] M. Kiwi, Exchange bias theory, J. Magn. Magn. Mater. **234**, 584 (2001).
[45] J. Guo, X. Zhao, Z. Lu, P. Shi, Y. Tian, Y. Chen, S. Yan, L. Bai, and M. Harder, Evidence for linear dependence of exchange bias on pinned uncompensated spins in an Fe/FeO bilayer, Phys. Rev. B **103**, 054413 (2021).